Supplemental material to the article "Redistribution of matter of a submicron silver film caused by femtosecond laser pulse"

Dynamic behavior. List of movies. Dynamics of (1) inflation of cupola, (2) capillary deceleration, (3) concentration of mass near the tip of cupola as a result of deceleration, (4) jet formation and growth, (5) formation of the droplet in the tip of the jet, (6) diffusion limited freezing of liquid into solid going from the edge of cupola up to the tip droplet, (7) elastic oscillations of the solidified structure and plastic decay of oscillations – all those processes and their interplay are demonstrated in the movie **220.** This is the case shown in Fig. 4a1, a2 of the main text. It corresponds to the experimental situation in Fig. 1.

In the experimental situation in Fig. 2, the processes (1–5) together with moderately delayed crystallization (6) take place. They are shown in the movie **225,** see also Fig. 4b1, b2. The delayed solidification is not able to prevent strong elongation of the jet. The long thin jet decays to the chain of droplets through Plateau–Rayleigh instability. The structure remaining on a surface consists from the cupola and the thin, rather long, sharply pointed jet.

Formation of nanocrown shown in Figures 3 and 4c1, c2 of the main text is illustrated in the movie **226.** In this case the solidification is strongly delayed and surface tension is weak. Thus a high liquid cupola flying away is formed. Late capillary deceleration forms a jet which decays into droplets with a very large first one. The solidification is so late that it doesn't stop not only decay of the jet but also decay of a cupola itself. Thus the upper part of cupola decays and only the bottom part of cupola survives thanks to solidification. Intermediate structure (in the movie **226**) with a mosaic of holes in the cupola shell around the jet resembles the mosaic around the jet visible in Fig. 4d in paper [20] cited in the main text.

Content. Let's consider (i) absorption of a laser light, (ii) heating and melting, and (iii) separation velocity from a substrate of a silver film exposed to action of a femtosecond (fs) laser pulse. Capillary and freezing scaling parameters are given in Section (iv). After that calculation of the mass distribution function (resolidification) for the modified structure is presented in Section (v).

(i) Absorption. We have to know absorption to calculate absorbed energy F_{abs} during fs pulse. This is necessary for definition of velocity of a film $v_{cm}(F_{abs})$ after its separation from a substrate.

For such metals as Ag, Au, and Cu an absorption coefficient $A = 1 - R$ is small for wavelengths longer than their d-band absorption edge, here R is a reflection coefficient. Absorption strongly depends on the surface conditions. For wavelength 515 nm used in our experiments, the coefficient $A = 1.7\,\%$ for Ag at normal incidence according to Johnson, Christy, "Optical constants of the noble metals," Phys. Rev. B **6**, 4370 (1972) and Babar, Weaver, "Optical constants of Cu, Ag, and Au revisited," Appl. Optics **54**, 477 (2015), while $A = 5\,\%$ according to Palik, "Handbook of Optical Constants of Solids" (Academic, 1985) and A is near to $7\,\%$ in Hagemann et al., "Optical constants from the far infrared to the x-ray region: Mg, Al, Cu, Ag, ...," J. Opt. Soc. Am. **65**, 742 (1975). These values differ four (!) times. Coefficient $A = 1.7\,\%$ corresponds to an ideal crystal, while $A = (5{-}7)\,\%$ – to real matter. Chemical impurities increase absorption.

Submicron Ag film packed from the nanocrystallite net visible in the SEM images is employed in the experiments described in the main text, see Figures 1–3. The film is fabricated by magnetron

sputtering. Reflectance of this film may be even more worse than $A = (5 \div 7)\,\%$.

Another reason which may cause enhancement of absorption is increase of the absorption coefficient $A(t) = \Phi[I_{inc}(t)]$ during a fs pulse $I_{inc}(t)$; here $I_{inc}(t)$ is a function describing temporal dependence of intensity of the incident pulse. This is the phenomenon of the nonlinear absorption. For a Gaussian pulse $I_{inc}(t) = I_0 \exp(-t^2/\tau_L^2)$ we can write $A = A(t; I_0, \tau_L)$ or $A = A(t; F_{inc}, \tau_L)$ instead of the functional $\Phi[I_{inc}(t)]$; here $F_{inc} = \sqrt{\pi} I_0 \tau_L$. The functional depends not only on current instant t and parameters I_0 (maximum intensity), τ_L but also on a shape of the function $I_{inc}(t)$.

Integral absorption $A = F_{abs}/F_{inc}$ is important for us since all durations (t_{ehc}, t_{eq}, t_s) are much longer than duration of a fs pulse τ_L. Significant increase (few %) of A for gold and wavelength λ begins near intensity $I_0 \approx 0.5 \div 1\,\mathrm{J/cm^2}$, see, papers Inogamov et al., "Nanospallation induced by an ultrashort laser pulse", JETP **107**, 1 (2008) [$\lambda = 1240\,\mathrm{nm}$] and Inogamov et al., "Two-temperature relaxation and melting after absorption of fs laser pulse," Appl. Surf. Sci. **255**, 9712 (2009); arXiv:0812.2965 [$\lambda_{probe} = 620\,\mathrm{nm}$].

For Ag and $\lambda = 800\,\mathrm{nm}$, according to Wai-Lun Chan et al., "Nonlinear energy absorption of fs laser pulses in noble metals", Appl. Ph. A **97**, 287 (2009), absorption increases from 1.6 % in the linear regime $F_{inc} < 250\,\mathrm{mJ/cm^2}$ to 2.5 % in nonlinear regime at $F_{inc} = 430\,\mathrm{mJ/cm^2}$. Transition from linear to nonlinear regime takes place at $\approx 250\,\mathrm{mJ/cm^2}$. This value corresponds to $\approx 60\,\%$ of a melting threshold $F_{inc}|_m = 430\,\mathrm{mJ/cm^2}$, $F_{abs}|_m = 0.025\,F_{inc}|_m = 11\,\mathrm{mJ/cm^2}$ for a bulk Ag; 400 nm film may be regarded as a bulk target when we consider the problem of absorption and heating. It is unclear, how Wai-Lun Chan et al. (2009) define the onset of melting. Their value $F_{abs}|_m = 11\,\mathrm{mJ/cm^2}$ looks as undersized. Melting threshold for the bulk target is larger than a melting threshold for a film thinner than thickness d_T of the heat affected zone. Our 100 nm film is thinner than d_T. Beginning of partial melting for our film corresponds to $23\,\mathrm{mJ/cm^2}$, see Section ii below.

Values of A from reference books for Ag and $\lambda = 800\,\mathrm{nm}$ vary from $A = 0.6\,\%$ (Babar, Weaver, 2015) to 1.5 % (Hagemann et al., 1975). These values are presented here to compare with $A = 1.6\,\%$ in linear regime in Wai-Lun Chan et al. (2009).

Similar problem of shortage of absorbed energy F_{abs} for melting is present in Ref. [7] of the main text: $19\,\mathrm{mJ/cm^2}$ are necessary for total melting of 50 nm gold film. While there is only $8\,\mathrm{mJ/cm^2}$ absorbed for the shot with $F_{inc} = 160\,\mathrm{mJ/cm^2}$ in [7] if we suppose the highest value of coefficient A.

Let's mention that in [7] gold is strongly mechanically coupled to substrate (through the intermediate 5 nm Cr layer). We can show that in this case the regimes with nanobump formation shown in Figs. 1 and 2 of the main text are impossible. Only nanocrown like regime (as in Fig. 3) is present.

Taking into account considerations mentioned above, below we will vary A in the range 5−9 %, see Fig. i.

(ii) Melting. Figs. 2, 3, and 4 in the main text correspond to incident energies 370, 530, and $1050\,\mathrm{mJ/cm^2}$. These energies are presented by the colored filled circles in Fig. i. Their positions along the upper horizontal axis are 370, 530, and $1050\,\mathrm{mJ/cm^2}$. The ranges putted step below and colored to the same colors present the intervals of absorbed fluences $F_{abs} = AF_{inc}$, $A = 5 \div 9\,\%$. Values F_{abs} are measured along the bottom horizontal axis.

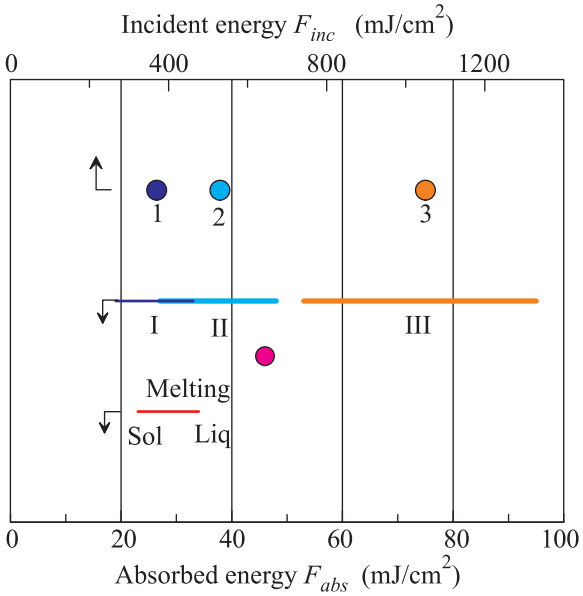

Fig. i. Values of incident and absorbed fluences relative to the melting range "melting". Incident values (the filled circles 1, 2, and 3) relate to Figures 2, 3, and 4. They are given at the upper horizontal axis. Colors link the filled circles 1, 2, and 3 with the corresponding ranges I, II, and III of absorbed fluences F_{abs}. These ranges appear thanks to uncertainty in absorption coefficient $A = 5 \div 9\,\%$, see text for explanations. The bottom horizontal axis gives F_{abs}

The range "melting" of the values F_{abs} in Fig. i represents the beginning and the end of the melting process. The points "sol" and "liq" are shown also in Fig. ii. They are cross-sections of the solidus "s" and liquidus "l" with the binodal curve "b". The estimate of $F_{abs} \approx 46\,\mathrm{mJ/cm^2}$ in Fig. ii for the magenta filled circle shown in Figs. i and ii is $F_{abs} = [C\,(1685 - 300) + q]h$, where $C \approx 3nk_B$, is heat capacity, 1685 and 300 are temperatures in K in the magenta circle and the "rt" point in Fig. ii, $q = 11.3\,\mathrm{kJ/mol}$ is heat of fusion for Ag, and $h = 100\,\mathrm{nm}$ is initial thickness of an Ag film. A film melts in a rarefaction wave (if there are enough energy: $F_{abs} > 23\,\mathrm{mJ/cm^2}$) if $F_{abs} < 46\,\mathrm{mJ/cm^2}$. Values F_{abs} for the points "sol" and "liq" in Fig. i are $C(1235-300)h \approx 23\,\mathrm{mJ/cm^2}$ and $[C(1235 - 300) + q]h \approx 34\,\mathrm{mJ/cm^2}$.

Our 100 nm thick film is thin relative to the thickness d_T of a heat affected zone in bulk Ag. This thickness is defined by enhanced (relative to the usual one-temperature $T = T_e = T_i$ value) electron heat conduction (ehc). Therefore in $t_{ehc} \approx 1 \div 2\,\mathrm{ps}$ after a fs pulse the electron temperature T_e equalizes spatially along thickness of a film. In a few ps after the T_e equalization along thickness, the T_e and T_i also become approximately equal to each other in the process of electron-ion energy exchange. Duration of this process is $t_{eq} \approx 4 \div 5\,\mathrm{ps}$. Both these durations are shorter than the sonic time scale $t_s = h/c_s \approx 30\,\mathrm{ps}$. Therefore if energy F_{abs} is less than $46\,\mathrm{mJ/cm^2}$ (but more than $23\,\mathrm{mJ/cm^2}$) then Ag melts at a time scale $\sim t_s$ thanks to volume expansion.

Temperature distribution is homogeneous across the thickness (heat conduction is switched off), thus Ag expands conserving local entropy. Example of an expansion trajectory is shown in Fig. ii as the brown dashed line between the magenta filled circle and the deep blue filled circle. During expansion the temperature drops from 1685 to 1600 K, density $10.49 \to 9\,\mathrm{g/cc}$, pressure drops from

11 GPa to almost zero value. The density drop $\Delta\rho$ is found from $c_s^2 = dp/d\rho \approx \Delta p/\Delta\rho$, with $c_s = 2.7\,\mathrm{km/s}$ for liquid Ag and $\Delta p = 11\,\mathrm{GPa}$. Of course, energy F_{abs} should be above the limit $F_{abs} \approx 23\,\mathrm{mJ/cm^2}$ to have a finite portion of liquid in the liquid-solid mixture. We see, that the experiments corresponding to Figs. 2 and 3 from the main text are near the melting region.

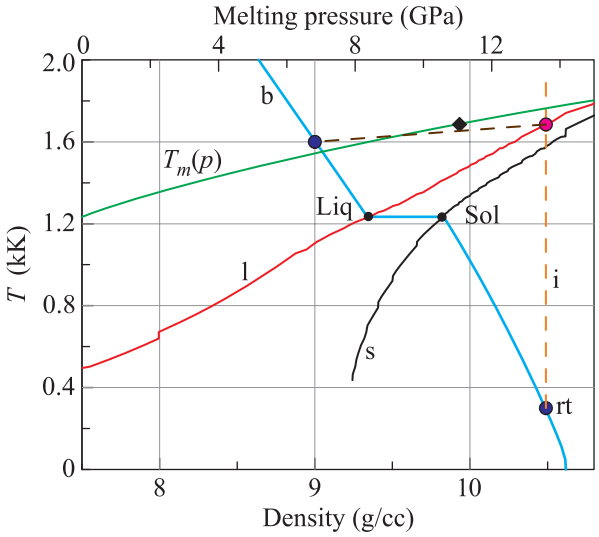

Fig. ii. Thermodynamics of Ag and hydrodynamics of heating and expansion. "b" is a coexistence curve (binodal), "s", "l" are solidus and liquidus. They bound the melting strip. $T_m(p)$ is a melting curve, $T_m(0) = 1.235\,\mathrm{kK}$. "rt" is the room temperature point. The magenta filled circle corresponds to intersection of the initial isochor "i" $10.49\,\mathrm{g/cc}$ and liquidus "l". Pressure in this intersection is 11 GPa (filled rhombus at the curve $T_m(p)$). Ag from the magenta circle expands along the brown dashed line. This is an adiabatic curve

(iii) Separation process. Duration 200 fs of a pulse used in our experiments is much shorter than durations $t_{ehc} < t_{eq} < t_s$ of the thermal and mechanical processes. There are a weak shock propagating in glass and two rarefaction waves running inside a film from the vacuum boundary of a silver film and from the contact boundary (CB) between Ag and glass. Pressure $p_{CB} = 0.24p$ at the contact is significantly lower than pressure p inside a film at the time interval $t_{eq} < t < t_s/2$. For our range of fluences the pressure p is weak relative to a bulk modulus $B = 100\,\mathrm{GPa}$ of Ag. Therefore linear acoustics is valid and we have: $p_{CB} = Z_g u_{CB} = pZ_g/(Z_A + Z_g) = 0.24p$; $Z_g = \rho_g c_g$, $Z_A = \rho_A c_A$ are acoustic impedances of glass and Ag; $\rho_g = 2.51\,\mathrm{g/cc}$, $c_g = 4\,\mathrm{km/s}$, $\rho_A = 10.49\,\mathrm{g/cc}$, $c_A = 3.1\,\mathrm{km/s}$ (plastic speed of sound in solid Ag); $u_{CB} = p/(Z_A + Z_g) = 230\,(p/10\,[\mathrm{GPa}])\,\mathrm{m/s}$ is velocity of the contact for $t < t_s$.

Ag film is weakly mechanically connected to the glass support. Therefore the film separates from substrate when a tensile part of the rarefaction wave propagating from the vacuum boundary comes to the contact; compare with mentioned above paper [7] with a film strongly connected to substrate. Contact pressure p_{CB} accelerates a film during a time interval t_s. Separation velocity $u_{cm} = p_{CB}/Z_A = 70(p/10\,[\mathrm{GPa}])\,\mathrm{m/s}$ is defined by the momentum balance $\rho_A h, u_{cm} = p_{CB} t_s$. Pressure p inside a film is defined by absorbed energy $p = \Gamma E = \Gamma F_{abs}/h \approx 0.27\,(F_{abs}/1\,[\mathrm{mJ/cm^2}])\,\mathrm{GPa}$, where $\Gamma \approx 2.7$ is Gruneisen parameter for solid Ag, E is internal energy per unit of volume, $h = 100\,\mathrm{nm}$. Combining

$u_{cm} \propto p$ and $p \propto F_{abs}$ we obtain velocity $u_{cm} \approx 1.9\,(F_{abs}/1\,[\mathrm{mJ/cm^2}])\,\mathrm{m/s}$ of a film after separation. Thus the highest ($A = 9\%$) velocities for the cases 1, 2, and 3 shown in Fig. i are: 63, 93, and 180 m/s, respectively.

(iv) Double scaling. Two scaling parameters (capillary V_σ/V_{cm} and thermal V_χ/V_{cm}) are introduced in the main text. Coefficient of surface tension for Ag near melting temperature 1.235 kK is 900 dyn/cm. We take average (between the solid and liquid values) heat diffusion coefficient $\chi = 1.3\,\mathrm{cm^2/s}$. Radiuses R_{cup} of the experimental cupolas are 1, 1.6, and 2.6 microns for the cases 1, 2, and 3 shown in Figure i and Figures 1, 2, and 3 of the main text. Then the scaling pairs (V_σ/V_{cm}, V_χ/V_{cm}; $v_\chi = \chi/R_{cup}$) are (0.9, 2), (0.6, 0.9), and (0.3, 0.3) for the experimental cases 1, 2, and 3. While the corresponding simulation pairs for the cases 1, 2, and 3 in Fig. 4 of the main text are (0.4, 0.2), (0.2, 0.2), and (0.2, 0.1). Thus we see that the experimental and simulation pairs are of the same order, but in simulation the velocities v_{cm} are 2–5 times higher.

(v) Density profile. Figures 4a1, b1, c1 in the main text present instant positions of the matter points in 3D space. The green cupola in Fig. iii shows a cross-section of the cupola from Fig. 4b1. We see the shell and the empty cavity under the shell.

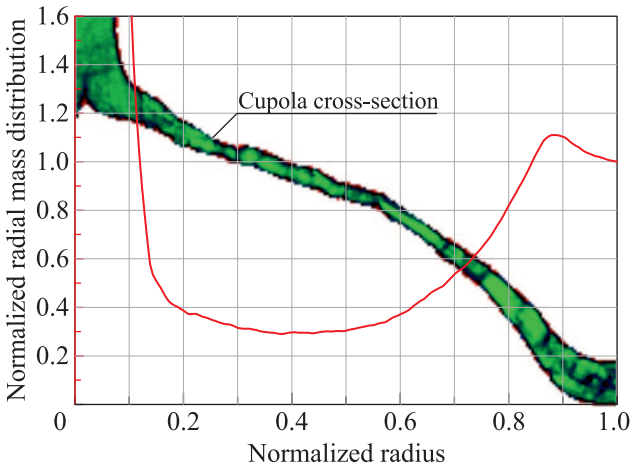

Fig. iii. Frozen cupola shape for the case 2 presented in Fig. 4b1, b2. This is the cross section of the cupola by a plane passing from the rotation symmetry axis (vertical axis). Green colors correspond to solid states. Thin dark lines and curves inside the solid mark crystalline domain boundaries. The cupola is shown in 1:1 vertical to horizontal scale ratio. The red curve is a radial normalized mass distribution $H(r)$ averaged along the azimuthal angle. It is obtained from the local density distribution $M(x, y)$ shown in Fig. 4b2 of the main text, see text for explanations

The red curve in Fig. iii is linked to the 2D density distribution $M(x, y, t) = \int_{-\infty}^{\infty} \rho(x, y, z, t)\, dz$ in Fig. 4b2, here integral is taken along the silver atoms, ρ is density of silver, x, y are axes in the plane of a target, and z is directed along the normal to the plane $z = 0$. The red curve gives averaged $M(r, t) = (1/2\pi) \int_0^{2\pi} M(r, \phi, t)\, d\phi$ and normalized distribution $H(r, t) = M(r, t)/\rho\, h$, where $M(r, \phi, t) = M(x, y)$, r, ϕ are polar coordinates in the plane $z = 0$, $\rho = 10.49\,\mathrm{g/cc}$ is solid state density of Ag, $h = 100\,\mathrm{nm}$ is initial thickness of a Ag film.

Evolution of the profile $H(r, t)$ starts from $H(r, t = -\infty) \equiv 1$. Maximum intensity of a fs pulse comes at $t = 0$ to the plane $z = 0$. Late in time cupola is frozen, becomes unmoved, thus the final

profile $H(r) \equiv H(r, t = \infty)$ is established. This profile is given in Fig. iii as the red curve.

The distribution $H(r)$ is proportional to the experimental distributions shown in Figures 1c and 2c as the black and green fluctuating curves and shown in Fig. 3c as the black and red fluctuating curves.

The distribution $H(r)$ in Fig. iii equals to 1 at the edge $r = R/R_{cup} = 1$ because here a film is unperturbed by laser action and therefore keeps its initial thickness and remains lying horizontally on the substrate. Slightly to the left from the point $r = 1$ the distribution $H(r)$ begin to increase. This increase is caused by the turn of the film, now separated from a substrate. The increase is finished when effect of stretching and thinning of a film overcomes effect of the turn of a film near the edge of a cupola. Further the function $H(r)$ decreases due to thinning of the cupola shell. At last the function $H(r)$ begins increase fast near the center. This is a result of formation of a jet.